

# On the near-threshold peak structure in the differential cross section of $\phi$ -meson photoproduction: indication of a missing resonance with non-negligible strangeness content

Alvin Kiswandhi and Shin Nan Yang

*Center for Theoretical Sciences, National Taiwan University, Taipei 10617, Taiwan*

*Department of Physics, National Taiwan University, Taipei 10617, Taiwan*

(Dated: April 6, 2019)

The details of the analysis of the near-threshold bump structure in the forward differential cross section of the  $\phi$ -meson photoproduction to determine whether it is a signature of a resonance, together with more extensive results, are presented. The analysis is carried out in an effective Lagrangian approach which includes Pomeron and  $(\pi, \eta)$  exchanges in the  $t$  channel, and contributions from the  $s$ - and  $u$ -channel excitations of a postulated nucleon resonance. In addition to the differential cross sections, we use the nine spin-density matrix elements as recently measured, instead of the  $\phi$ -meson decay angular distributions which depend only on six spin-density matrix elements as was done before, to constrain the resonance parameters. We conclude that indeed the nonmonotonic behavior, along with the other experimental data as reported by LEPS, can only be explained with an assumption of the excitation of a resonance of spin  $3/2$ , as previously reported. However, both parities of  $(\pm)$  can account for the data equally well with almost identical mass of  $2.08 \pm 0.04$  GeV and width of  $0.501 \pm 0.117$  and  $0.570 \pm 0.159$  for  $3/2^+$  and  $3/2^-$ , respectively. The ratio of the helicity amplitudes  $A_{\frac{1}{2}}/A_{\frac{3}{2}}$  calculated from the resulting coupling constants differs in sign from that of the known  $D_{13}(2080)$ . More experimental data on single and double polarization observables are needed to resolve the parity. We further find that with an assumption of large values of the OZI-evading parameters  $x_{\text{OZI}} = 12$  for  $J^P = 3/2^-$  and  $x_{\text{OZI}} = 9$  for  $J^P = 3/2^+$ , the discrepancy between the recent experimental data on  $\omega$ -meson photoproduction and theoretical model can be considerably reduced. We argue that the large value of  $x_{\text{OZI}}$  indicates that the postulated resonance contains non-negligible amount of strangeness content.

PACS numbers: 13.60.Le, 25.20.Lj, 14.20.Gk

## I. INTRODUCTION

The  $\phi$ -meson photoproduction reaction has long been extensively studied. At high energy, diffractive process dominates and it can be well described by  $t$ -channel Pomeron ( $P$ ) exchange [1, 2]. In the low-energy region, the nondiffractive processes of the pseudoscalar  $(\pi, \eta)$ -meson exchanges are also known to contribute [1]. Other processes, such as nucleon exchange [3, 4], nucleon resonances [5, 6], second Pomeron exchange,  $t$ -channel scalar meson and glueball exchanges [6, 7], and  $s\bar{s}$ -cluster knockout [4, 8, 9] have also been investigated. However, a peak in the differential cross sections of  $\phi$  photoproduction on protons at forward angles around  $E_\gamma \sim 2.0$  GeV as recently observed by the LEPS collaboration [10] cannot be explained by the processes mentioned above.

Since a bump in the cross sections is often associated with excitation of resonances, it is then tempting to see if the peak observed in Ref. [10] can be described by a resonance. There exist previous works studying the effects of resonances in  $s$  and  $u$  channels with masses up to 2 GeV [5, 6]. Ref. [5] employs  $SU(6) \otimes O(3)$  symmetry within a constituent quark model and included explicitly excited resonances with quantum numbers  $n \leq 2$ . On the other hand, Ref. [6] includes all the known 12 resonances below 2 GeV listed in Particle Data Group [11], with coupling constants determined by available experimental data [12, 13] at large momentum transfers. The

resonances are found to play significant roles in the polarization observables. Nevertheless, the resonances considered, either listed in PDG table or predicted by some quark model, cannot account for the nonmonotonic behavior as reported in Ref. [10].

In Ref. [14], we have tried to explore the possibility on whether such a nonmonotonic behavior could be explained by a postulated resonance by fiat in the neighborhood of observed peak position. We found that, with an addition of a resonance of spin  $3/2$  to a background mechanism which consists of Pomeron and  $(\pi, \eta)$ -meson exchanges in  $t$ -channel, not only the peak in the forward differential cross section but also the  $t$  dependence of differential cross section (DCS) and  $\phi$  meson decay angular distribution can be well described. Similar attempt was also made in Ref. [15], where the effect of the  $K\Lambda(1520)$  is taken into account in a coupled-channel analysis. Their results preferred a resonance of  $J^P = 1/2^-$ . However, the calculation is marred by a mistake in the phase of the Pomeron amplitude.

In this paper, we give the details of our previous analysis [14] and present more extensive results of our calculation. In addition, we employ the new LEPS data [16] which consist of nine spin-density matrix elements measured at three different energies to determine the resonance parameters, instead of the decay angular distributions of the  $\phi$  meson, which involve only six spin-density matrix elements, taken only at two energies given in Ref.

[10], as was done before. The use of a larger data set with better precision should provide a more stringent constraint on the model and give rise to more reliable extracted resonance properties. We also provide an estimation of the strangeness content of the postulated resonance.

This paper is organized as follows. The model used in our analysis, which consists of Pomeron and  $(\pi, \eta)$ -meson exchanges in  $t$  channel, and a postulated resonance is given in Sec. II. The extracted resonance parameters, their possible effects in the polarization observables and  $\omega$  photoproduction, as well as an estimation of the strangeness content of the resonance, are presented in Sec. III. The summary is given in Sec. IV.

## II. THE MODEL FOR $\phi$ MESON PHOTOPRODUCTION

We first introduce the kinematic variables  $k$ ,  $p_i$ ,  $q$ , and  $p_f$  for the four-momenta of the incoming photon, initial proton, outgoing  $\phi$ -meson, and final proton, respectively, with  $s = (k + p_i)^2 = (q + p_f)^2$ ,  $t = (q - k)^2 = (p_f - p_i)^2$ , and  $u = (p_f - k)^2 = (q - p_i)^2$ .

We follow the convention of PDG [11] and define the invariant amplitude  $-i\mathcal{M}$  as related to the  $S$ -matrix by

$$S_{fi} = \delta_{fi} - i \frac{(2\pi)^4 \delta^{(4)}(p_f + q - p_i - k)}{(2E_{\mathbf{p}_f})^{1/2} (2E_{\mathbf{p}_i})^{1/2} (2E_{\mathbf{q}})^{1/2} (2E_{\mathbf{k}})^{1/2}} \mathcal{M}_{fi}, \quad (1)$$

with normalization  $\langle p_f | p_i \rangle = (2\pi)^3 \delta^{(3)}(\mathbf{p}_f - \mathbf{p}_i)$  for free-particle momentum state and  $\bar{u}(p, s)u(p, s) = 2m$  for Dirac spinor with mass  $m$ . In addition to the background mechanism of Pomeron-exchange,  $t$ -channel  $\pi$ - and  $\eta$ -exchange, we will postulate the existence of a resonance by fiat and see whether we could describe the data of LEPS [10, 16]. We can then write the full amplitude  $\mathcal{M}$  as

$$\mathcal{M}_{fi} = \mathcal{M}_P + \mathcal{M}_{\pi+\eta} + \mathcal{M}_{N^*}, \quad (2)$$

as shown in Fig. 1, where  $\mathcal{M}_{N^*}$  contains both  $s$ - and  $u$ -channel contributions. The unpolarized differential cross section is related to the invariant amplitude by

$$\frac{d\sigma}{dt} = \frac{1}{64\pi s |\mathbf{k}_{cm}|^2} \frac{1}{4} \sum_{\lambda_N, \lambda_\gamma} \sum_{\lambda_{N'}, \lambda_\phi} |\mathcal{M}_{fi}|^2, \quad (3)$$

with  $\mathbf{k}_{cm}$  is the photon three momentum in the center-of-mass (CM) frame and  $\lambda_N$ ,  $\lambda_{N'}$ ,  $\lambda_\gamma$  and  $\lambda_\phi$  denote the helicities of the initial proton, final proton, incoming photon, and outgoing  $\phi$ -meson, respectively.

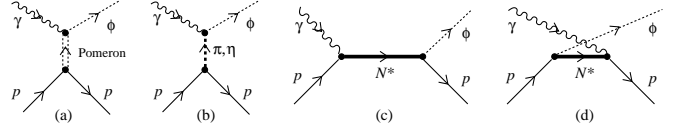


FIG. 1: Pomeron,  $(\pi, \eta)$  exchanges,  $s$ -,  $u$ -channel  $N^*$  excitation diagrams for  $\gamma p \rightarrow \phi p$  reaction are labeled (a), (b), (c), and (d), respectively.

### A. Pomeron exchange

Following Refs. [6, 17], we can easily write down the Pomeron-exchange amplitude of Fig. 1(d),

$$\mathcal{M}_P = -\bar{u}(p_f, \lambda_{N'}) M(s, t) \Gamma^{\mu\nu} u(p_i, \lambda_N) \times \varepsilon_\mu^*(q, \lambda_\phi) \varepsilon_\nu(k, \lambda_\gamma), \quad (4)$$

where  $\varepsilon_\mu(q, \lambda_\phi)$  and  $\varepsilon_\nu(k, \lambda_\gamma)$  are the polarization vectors of the  $\phi$ -meson and photon with  $\lambda_\phi$  and  $\lambda_\gamma$ , respectively, and  $u(p_i, \lambda_N)[\bar{u}(p_f, \lambda_{N'})]$  is the Dirac spinor of the nucleon with momentum  $p_i(p_f)$  and helicity  $\lambda_N(\lambda_{N'})$ . The transition operator  $\Gamma^{\mu\nu}$  in Eq. (4) is

$$\Gamma^{\mu\nu} = \left( g^{\mu\nu} - \frac{q^\mu q^\nu}{q^2} \right) \not{k} - \left( k^\mu - \frac{k \cdot q q^\mu}{q^2} \right) \gamma^\nu - \left( \gamma^\mu - \frac{\not{q} q^\mu}{q^2} \right) \left[ \not{q}^\nu - \frac{k \cdot q (p_i^\nu + p_f^\nu)}{k \cdot (p_i + p_f)} \right]. \quad (5)$$

The scalar function  $M(s, t)$  is described by the Reggeon parametrization,

$$M(s, t) = C_P F_1(t) F_2(t) \frac{1}{s} \left( \frac{s - s_{th}}{s_0} \right)^{\alpha_P(t)} \times \exp \left[ -\frac{i\pi}{2} \alpha_P(t) \right], \quad (6)$$

where the Pomeron trajectory is taken to be  $\alpha_P(t) = 1.08 + 0.25t$  and  $s_0 = (m_N + m_\phi)^2$ .  $F_1(t)$ , the isoscalar form factor of the nucleon and  $F_2(t)$ , the form factor of the  $\phi$ -photon-Pomeron coupling are given as [2, 6],

$$F_1(t) = \frac{4m_N^2 - a_N^2 t}{(4m_N^2 - t)(1 - t/t_0)^2}, \quad (7)$$

$$F_2(t) = \frac{2\mu_0^2}{(1 - t/m_\phi^2)(2\mu_0^2 + m_\phi^2 - t)}, \quad (8)$$

with  $\mu_0^2 = 1.1 \text{ GeV}^2$ ,  $a_N^2 = 2.8$ , and  $t_0 = 0.7 \text{ GeV}^2$ .

In this study, we follow Ref. [6] by choosing the strength factor  $C_P = 3.65$ , which is obtained by fitting to the total cross sections data at high energy, as shown in the upper figure in Fig. 2, where the inset show the enlarged view of the region for  $E_\gamma \leq 7 \text{ GeV}$ . We include a threshold factor  $s_{th}$  as was done in Refs. [3, 6] in order to get a better agreement with experimental data near the threshold region. If  $s_{th} = 0$  is chosen as done in Ref. [6], a problem arises. Namely, the results for forward differential cross sections would overestimate the

experimental data [18] by about 20% as seen in the lower figure of Fig. 2 around  $E_\gamma = 6$  GeV. Since pomeron properties and behaviors at lower energies are not well-established, we adjust this parameter to fit the experimental data on the differential cross sections around  $E_\gamma = 6$  GeV.  $E_\gamma = 6$  GeV is chosen because at this energy, one can reasonably expect that all other contributions from hadronic intermediate states would become negligible and only pomeron contributes. Furthermore, around this energy, experimental data are quite reliable in that they have relatively small error bars and rise steadily without much fluctuation. These give us confidence to match the pomeron contribution to the experimental data at this energy by fixing  $s_{th} = 1.3$  GeV<sup>2</sup>.

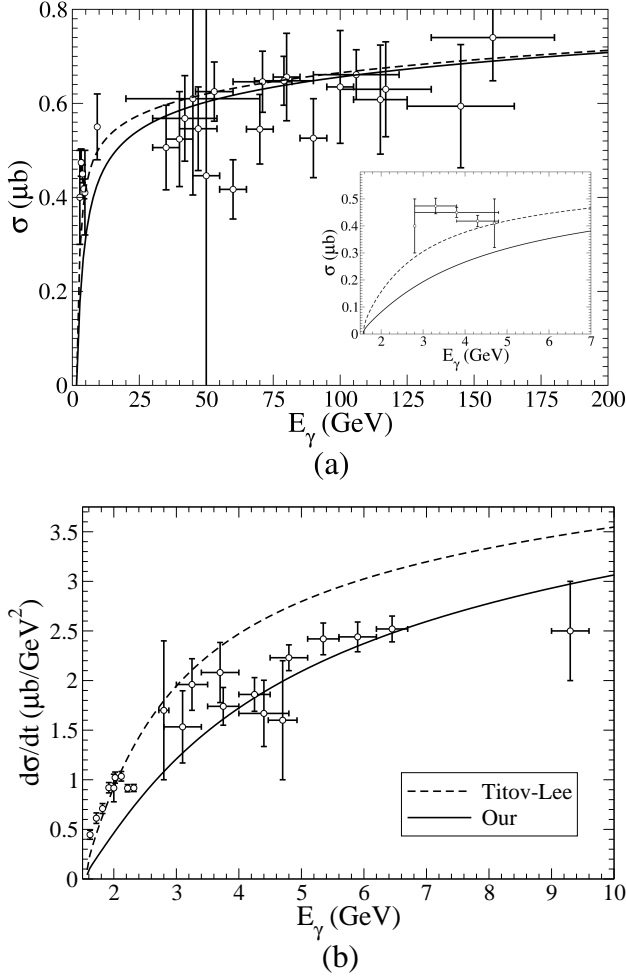


FIG. 2: (a) Total cross sections of  $\phi$  photoproduction as a function of photon lab energy  $E_\gamma$ . The inset gives an enlarged view for the region with  $E_\gamma \leq 7$  GeV. (b) Differential cross sections of  $\phi$  photoproduction at forward angle as a function of photon lab energy  $E_\gamma$ . Results of this work (Our) and Ref. [6] (Titov-Lee) are drawn as full and dashed lines, respectively. Data is taken from Ref. [18].

## B. $\pi$ and $\eta$ -meson exchanges

The amplitudes for the  $\pi$  and  $\eta$  exchanges in  $t$  channel, Fig. 1(c) in a straightforward manner [8, 9] and are given by

$$\begin{aligned} \mathcal{M}_{\pi+\eta} &= \frac{-eg_{\gamma\phi\pi}g_{\pi NN}F_\pi^2(t)}{m_\phi} \bar{u}(p_f, \lambda_{N'}) \gamma_5 \frac{\varepsilon^{\mu\nu\rho\sigma} q_\mu k_\rho}{t - m_\pi^2} \\ &\times u(p_i, \lambda_N) \varepsilon_\nu^*(q, \lambda_\phi) \varepsilon_\sigma(k, \lambda_\gamma) + \\ &- \frac{eg_{\gamma\phi\eta}g_{\eta NN}F_\eta^2(t)}{m_\phi} \bar{u}(p_f, \lambda_{N'}) \gamma_5 \frac{\varepsilon^{\mu\nu\rho\sigma} q_\mu k_\rho}{t - m_\eta^2} \\ &\times u(p_i, \lambda_N) \varepsilon_\nu^*(q, \lambda_\phi) \varepsilon_\sigma(k, \lambda_\gamma), \end{aligned} \quad (9)$$

with the coupling constants  $g_{\pi NN}$ ,  $g_{\gamma\phi\pi}$ , and  $g_{\gamma\phi\eta}$ , as well as the form factors  $F_\pi(t)$  and  $F_\eta(t)$  for the virtually exchanged mesons at the  $MNN$  and  $\gamma\phi M$  ( $M = \pi, \eta$ ) vertices, respectively, are taken to be the same as in Ref. [17]. We choose  $g_{\eta NN} = 1.12$  [19] and  $\Lambda_\pi = \Lambda_\eta = 1.2$  GeV which are slightly different with the values given in Ref. [17]. The choice of the cut-off parameter  $\Lambda_\pi = 1.2$  GeV would lead to a  $F_\pi(t)$  which agrees well with the  $\pi NN$  form factors as obtained in the meson-exchange  $\pi N$  model Ref. [20] in the region of  $-0.5 < t < 0$  GeV<sup>2</sup> where most of the data considered in this present work lie.

## C. Excitation of a baryon resonance

The Feynman diagrams with an  $N^*$  in the intermediate state in  $s$ - and  $u$ -channel are shown in Fig. 1(a) and (b). To evaluate the invariant amplitudes involving  $N^*$ , we use the following interaction Lagrangians. For the coupling of spin-1/2 and 3/2 resonances to  $\gamma N$ , we choose the commonly used interaction Lagrangians [19, 21, 22]

$$\begin{aligned} \mathcal{L}_{\gamma NN^*}^{1/2^\pm} &= eg_{\gamma NN^*}^{(2)} \bar{\psi}_N \Gamma^\pm \sigma_{\mu\nu} F^{\mu\nu} \psi_{N^*} + \text{h.c.}, \quad (10) \\ \mathcal{L}_{\gamma NN^*}^{3/2^\pm} &= ieg_{\gamma NN^*}^{(1)} \bar{\psi}_N \Gamma^\pm (\partial^\mu \psi_{N^*}^\nu) \tilde{F}_{\mu\nu} \\ &+ eg_{\gamma NN^*}^{(2)} \bar{\psi}_N \Gamma^\pm \gamma^5 (\partial^\mu \psi_{N^*}^\nu) F_{\mu\nu} + \text{h.c.}, \quad (11) \end{aligned}$$

where  $F_{\mu\nu} = \partial_\mu A_\nu - \partial_\nu A_\mu$  is the electromagnetic field tensor, and  $\sigma_{\mu\nu} = \frac{i}{2}(\gamma_\mu \gamma_\nu - \gamma_\nu \gamma_\mu)$ . Also,  $\tilde{F}_{\mu\nu} = \frac{1}{2}\epsilon_{\mu\nu\alpha\beta} F^{\alpha\beta}$  denotes the dual electromagnetic field tensor with  $\epsilon^{0123} = +1$ . The operator  $\Gamma^\pm$  are given by  $\Gamma^+ = 1$  and  $\Gamma^- = \gamma_5$ . For the  $\phi NN^*$  interaction Lagrangians, we have

$$\begin{aligned} \mathcal{L}_{\phi NN^*}^{1/2^\pm} &= g_{\phi NN^*}^{(1)} \bar{\psi}_N \Gamma^\pm \gamma^\mu \psi_{N^*} \phi_\mu \\ &+ g_{\phi NN^*}^{(2)} \bar{\psi}_N \Gamma^\pm \sigma_{\mu\nu} G^{\mu\nu} \psi_{N^*} + \text{h.c.}, \quad (12) \\ \mathcal{L}_{\phi NN^*}^{3/2^\pm} &= ig_{\phi NN^*}^{(1)} \bar{\psi}_N \Gamma^\pm (\partial^\mu \psi_{N^*}^\nu) \tilde{G}_{\mu\nu} \\ &+ g_{\phi NN^*}^{(2)} \bar{\psi}_N \Gamma^\pm \gamma^5 (\partial^\mu \psi_{N^*}^\nu) G_{\mu\nu} \\ &+ ig_{\phi NN^*}^{(3)} \bar{\psi}_N \Gamma^\pm \gamma^5 \gamma_\alpha (\partial^\alpha \psi_{N^*}^\nu - \partial^\nu \psi_{N^*}^\alpha) (\partial^\mu G_{\mu\nu}) \\ &+ \text{h.c.}, \quad (13) \end{aligned}$$

where  $G^{\mu\nu}$  is defined as  $G^{\mu\nu} = \partial^\mu \phi^\nu - \partial^\nu \phi^\mu$  with  $\phi^\mu$  the field of  $\phi$ -meson. The dual field tensor  $\tilde{G}_{\mu\nu}$  is again defined in the same way as its electromagnetic counterpart with  $F^{\alpha\beta} \rightarrow G^{\alpha\beta}$ . Notice that we could have chosen to describe the  $\gamma NN^*$  in the same way as we describe the  $\phi NN^*$  interactions. However, current conservation consideration fixes  $g_{\gamma NN^*}^{(1)}$  for  $J^P = 1/2^\pm$  resonances to be zero. In addition, the term proportional to  $g_{\gamma NN^*}^{(3)}$  in the Lagrangian densities of Eq. (13) vanishes in the case of real photon. With the Lagrangians given in Eqs. (11-13), the full invariant amplitude of  $s$  and  $u$  channels can readily be written down straightforwardly by following the Feynman rules.

The form factor for the vertices used in the  $s$ - and  $u$ -channel diagrams,  $F_{N^*}(p^2)$ , is taken to be similar as in Ref. [20]

$$F_{N^*}(p^2) = \frac{\Lambda^4}{\Lambda^4 + (p^2 - M_{N^*}^2)^2}, \quad (14)$$

with  $\Lambda$  is the cut-off parameter for the virtual  $N^*$ . In this work, we choose  $\Lambda = 1.2$  GeV for all resonances. The spin-1/2  $N^*$  propagator can be written in a Breit-Wigner form as

$$G^{(1/2)}(p) = \frac{i(\not{p} + M_{N^*})}{p^2 - M_{N^*}^2 + iM_{N^*}\Gamma_{N^*}}, \quad (15)$$

with  $\Gamma_{N^*}$  the total decay width of  $N^*$ . The Rarita-Schwinger propagator is used for the spin-3/2  $N^*$

$$G_{\mu\nu}^{(3/2)}(p) = \frac{i(\not{p} + M_{N^*})}{p^2 - M_{N^*}^2 + iM_{N^*}\Gamma_{N^*}} \left[ -g_{\mu\nu} + \frac{1}{3}\gamma_\mu\gamma_\nu - \frac{1}{3M_{N^*}^2}(p_\mu\gamma_\nu - p_\nu\gamma_\mu) + \frac{2}{3M_{N^*}^2}p_\mu p_\nu \right]. \quad (16)$$

Because  $u < 0$ , we take  $\Gamma_{N^*} = 0$  MeV for the propagator in the  $u$  channel.

It should, however, be stressed that, we do not know the value of the coupling constants  $g_{\phi NN^*}$  and  $g_{\gamma NN^*}$ , as our calculations are done in the tree level. Therefore, in present calculation, we show the values of  $g_{\gamma NN^*}g_{\phi NN^*}$  obtained by fitting the experimental data.

### III. RESULTS AND DISCUSSIONS

With the model presented in Sec. II, one can easily obtain the full amplitude of  $\gamma p \rightarrow \phi p$  reaction and calculate the scattering observables straightforwardly with a specific assignment of spin-parity of the resonance. Since the peak appears to lie close to the  $\phi N$  threshold, only the lower partial waves are important and we shall consider only  $J^P = 1/2^\pm, 3/2^\pm$  as the possible candidates for the spin-parity assignment of the resonance. In this work, we fit our model simultaneously to differential cross section at forward angle as a function of photon energy

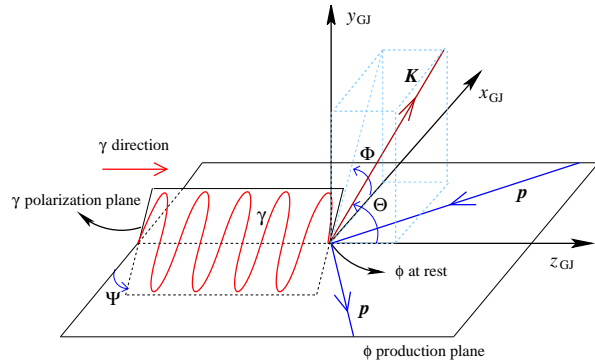


FIG. 3: (Color online) The  $\phi$  photoproduction in Gottfried-Jackson system.

and differential cross sections dependence on  $t$  at eight photon energies reported in Ref. [10], as well as to nine spin-density matrix elements  $\rho_{ij}^\alpha$  [23] as a function of  $t$  at three photon energies [16]. We use the Gottfried-Jackson system, in which  $\phi$ -meson is at rest, as depicted in Fig. 3, to analyze the spin-density matrix elements. The  $z_{GJ}$  axis is taken to be along the incoming photon momentum while  $y_{GJ}$  axis is taken to be along  $\mathbf{p}_f \times \mathbf{p}_i$  direction, with  $\mathbf{p}_f$  and  $\mathbf{p}_i$  the three-momentum of final and initial proton, respectively. The  $x_{GJ}$  axis is chosen to form a right-handed coordinate system.

Notice that in our previous work [14], decay angular distributions  $W$ , instead of the spin-density matrix elements  $\rho_{ij}^\alpha$  were used in the data set to which we fit our model parameters. Even though the decay angular distributions are also functions of spin-density matrix elements (SDME), they depend only on only six out of a total of nine SDMEs. Furthermore, the decay angular distributions used in Ref. [14], as presented in Ref. [10], are taken only at two photon energies and averaged over  $t$ , while the nine SDMEs used in this work as presented in Ref. [16] are taken at three photon energies and are functions of  $t$ . We expect that the larger set of data considered in this work would provide a more stringent constraint on our model and results.

In tree-level approximation, only products like  $g_{\gamma NN^*}g_{\phi NN^*}$  enter. The other parameters in our model are the resonance mass and width. They are determined with the use of MINUIT by fitting to the data measured at SPring8 [10, 16] as described in the previous paragraphs.

We find that, with assignments of spin-parity  $J^P = 1/2^\pm$  for the resonance, the nonmonotonic behavior in the forward differential cross-section near threshold can be explained only with considerably stronger resonance contributions. As a result, the differential cross section as a function of  $t$ , as well as spin-density matrix elements, would be in disagreement with the experimental data [10, 16]. The resulting  $\chi^2/N$  from such fit will be around  $5 \sim 9$ , which is definitely far above those obtained by

TABLE I: The  $N^*$  parameters for  $J^P = 3/2^\pm$  resonances together with their errors obtained by HESSE method of MINUIT package.

	$J^P = 3/2^+$	$J^P = 3/2^-$
$M_{N^*}$ (GeV)	$2.08 \pm 0.04$	$2.08 \pm 0.04$
$\Gamma_{N^*}$ (GeV)	$0.501 \pm 0.117$	$0.570 \pm 0.159$
$eg_{\gamma NN^*}^{(1)} g_{\phi NN^*}^{(1)}$	$0.003 \pm 0.009$	$-0.205 \pm 0.083$
$eg_{\gamma NN^*}^{(1)} g_{\phi NN^*}^{(2)}$	$-0.084 \pm 0.057$	$-0.025 \pm 0.017$
$eg_{\gamma NN^*}^{(1)} g_{\phi NN^*}^{(3)}$	$0.025 \pm 0.076$	$-0.033 \pm 0.017$
$eg_{\gamma NN^*}^{(2)} g_{\phi NN^*}^{(1)}$	$0.002 \pm 0.006$	$-0.266 \pm 0.127$
$eg_{\gamma NN^*}^{(2)} g_{\phi NN^*}^{(2)}$	$-0.048 \pm 0.047$	$-0.033 \pm 0.032$
$eg_{\gamma NN^*}^{(2)} g_{\phi NN^*}^{(3)}$	$0.014 \pm 0.040$	$-0.043 \pm 0.032$
$\chi^2/N$	0.891	0.821

fitting using  $J^P = 3/2^\pm$  resonances, as seen in Table I. Therefore, we conclude that spin-1/2 resonance cannot fit the experimental data. It is worthwhile to note that in the constituent quark model of Refs. [24, 25], spin-1/2 resonances are also not predicted to be of significant contribution at around  $E_\gamma = 2$  GeV. Our results seem to be in line with their prediction.

On the other hand, we find that the experimental data can be well described with a spin-parity assignment of either  $J^P = 3/2^-$  or  $J^P = 3/2^+$  for the postulated resonance. In the following, we first present our model predictions for the differential cross sections, spin-density matrix elements, and decay angular distributions and compare them with the data for both the cases with  $3/2^-$  and  $3/2^+$  resonances. We then present an analysis on the composition of the bump structure. After that, we proceed by predicting the effect on  $\omega N$  channel and estimating the strangeness content of the resonance. Lastly, we present also some predictions on the polarization observables.

#### A. Differential cross sections, spin-density matrix elements, and decay angular distributions

The quality of the agreement between data and model predictions for both spin-parity assignments, i.e.,  $3/2^\pm$ , is similar even though the resulting  $\chi^2$  value is slightly smaller for the case  $J^P = 3/2^-$  as seen in Table I where the values of the products of  $g_{\gamma NN^*} g_{\phi NN^*}$  are also presented. The obtained values for the mass and width for  $3/2^-$  and  $3/2^+$  resonances are very close, i.e., (mass, width) of (2.08, 0.570) and (2.08, 0.501) GeV, respectively, however, the products of the coupling constants are quite different.

The results of our best fit, as compared to the data of Refs. [10, 16], are shown in Fig. 4–8. The dotted lines represent the contributions of the background of pomeron plus ( $\pi, \eta$ ) exchanges and the solid and dashed curves correspond to the full model predictions including

a resonance of  $3/2^-$  and  $3/2^+$ , respectively. In Figs. 4 and 5, the forward differential cross section as function of energy, where a bump is observed, and the differential cross section as function of  $t$  are shown, respectively. The contribution of the resonance alone is also shown therein with dash-dotted and dash-dot-dotted lines corresponding to  $3/2^-$  and  $3/2^+$ , respectively. We see that besides producing a bump in the forward differential cross

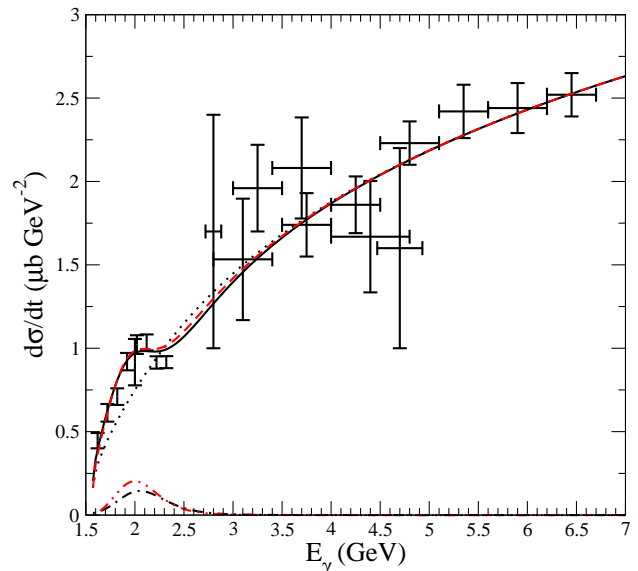


FIG. 4: (Color online) The results obtained by employing a  $J^P = 3/2^\pm$  resonances in our model for differential cross section of  $\gamma p \rightarrow \phi p$  at forward direction as a function of the incoming photon energy  $E_\gamma$ . Data are taken from Ref. [18]. The dotted lines represent the background which includes pomeron- and meson-exchange contributions only. The full and dashed lines are the total contributions including  $J^P = 3/2^-$  and  $J^P = 3/2^+$  resonances, respectively. The dash-dotted and dash-dot-dotted lines denote the resonant  $s$ - and  $u$ -channel contributions of  $J^P = 3/2^-$  and  $J^P = 3/2^+$  resonances, respectively.

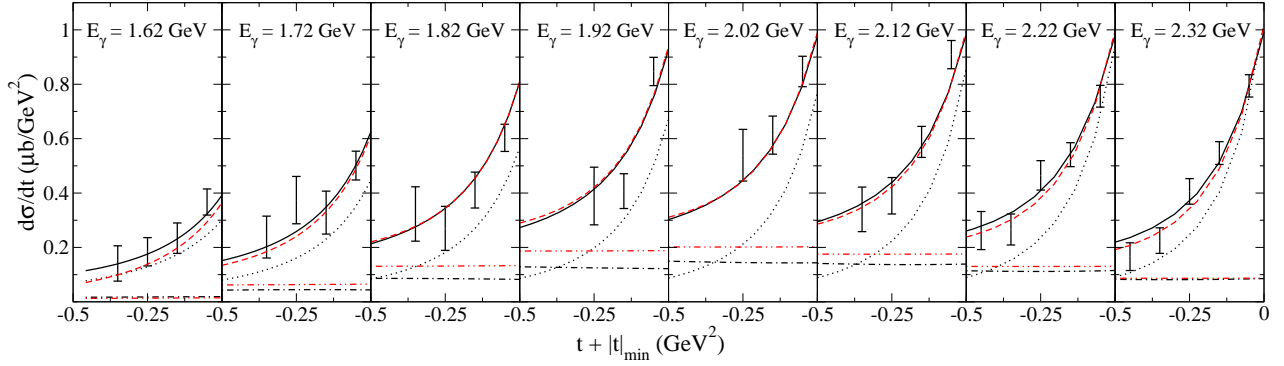


FIG. 5: (Color online) The results obtained for differential cross section of  $\gamma p \rightarrow \phi p$  as a function of  $t + |t|_{\min}$  at eight different photon energies  $E_\gamma$ , as given inside each plot. Data is taken from Ref. [18]. Notation is as in Fig. 4.

section, the resonance reduces the discrepancy between predictions of the background mechanisms and the data substantially in the  $t$  dependence of the differential cross sections.

In Figs. 6-8, our model predictions for the SDME's in the three energy regions of  $1.77 < E_\gamma < 1.97$  GeV,  $1.97 < E_\gamma < 2.17$  GeV, and  $2.17 < E_\gamma < 2.37$  GeV are shown together with the data of Ref. [16]. It is seen that in some cases, e.g.,  $\rho_{10}^0$ ,  $\rho_{10}^1$ ,  $\rho_{10}^2$  in  $1.97 < E_\gamma < 2.17$  GeV, the nonresonant contribution alone already describes well the data and the resonance contributions are small. However, there are several cases that a  $3/2^+$  resonance is indeed quite helpful to bridge the difference between background contribution and the data, especially for  $\rho_{00}^0$  in all energy regions, though its corrections are in the wrong direction

for  $\rho_{1,-1}^1$  and  $\rho_{1,-1}^2$  in the region of  $1.77 < E_\gamma < 1.97$  GeV. The effect of a  $3/2^-$  resonance is in general less conspicuous than that of a  $3/2^+$  resonance.

The decay angular distributions  $W(\cos \Theta)$ ,  $W(\Phi - \Psi)$ ,  $W(\Phi)$ ,  $W(\Phi + \Psi)$ , and  $W(\Psi)$  in Gottfried-Jackson frame depend on six SDMEs via the following relations,

$$W(\cos \Theta) = \frac{3}{2} \left[ \frac{1}{2} (1 - \rho_{00}^0) \sin^2 \Theta + \rho_{00}^0 \cos^2 \Theta \right],$$

$$W(\Phi) = \frac{1}{2\pi} (1 - 2\text{Re}\rho_{1,-1}^0 \cos 2\Phi),$$

$$W(\Phi - \Psi) = \frac{1}{2\pi} \{1 + 2P_\gamma(\rho_{1,-1}^1 - \text{Im}\rho_{1,-1}^2) \times \cos[2(\Phi - \Psi)]\},$$

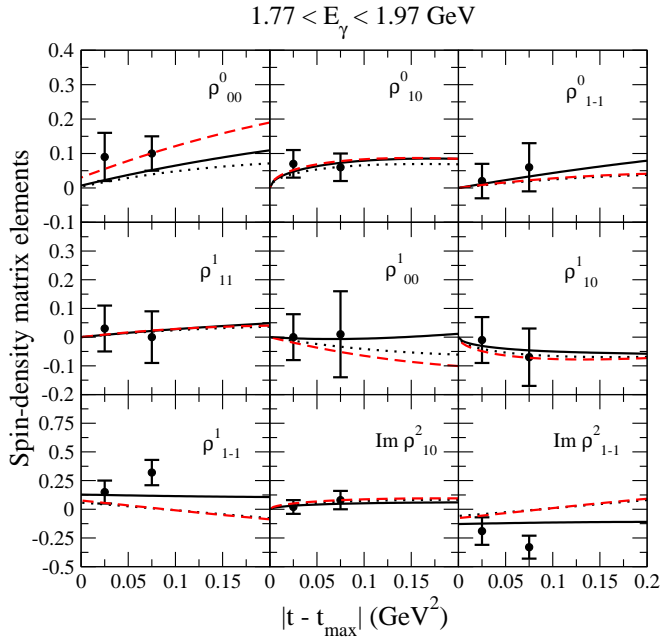


FIG. 6: (Color online) Spin-density matrix elements  $\rho_{ij}^\alpha$  in Gottfried-Jackson system as a function of  $t$  at  $1.77 < E_\gamma < 1.97$  GeV. Notation is as in Fig. 4.

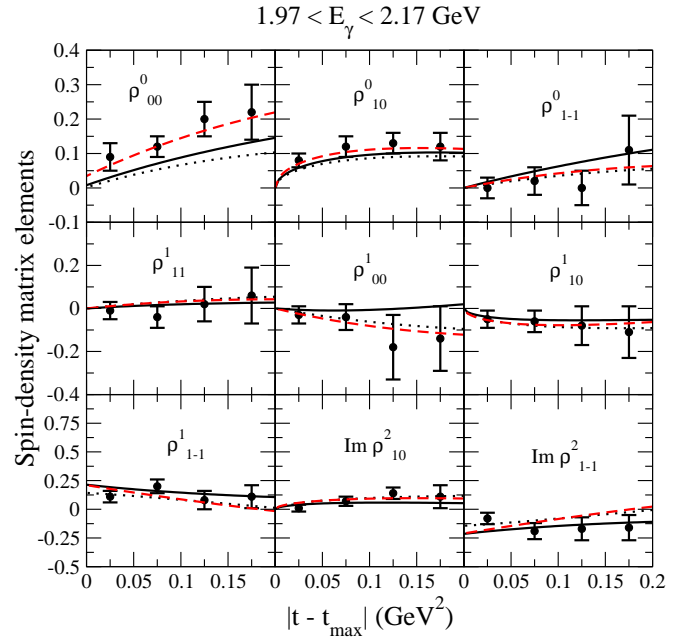


FIG. 7: (Color online) Spin-density matrix elements  $\rho_{ij}^\alpha$  in Gottfried-Jackson system as a function of  $t$  at  $1.97 < E_\gamma < 2.17$  GeV. Notation is as in Fig. 4.

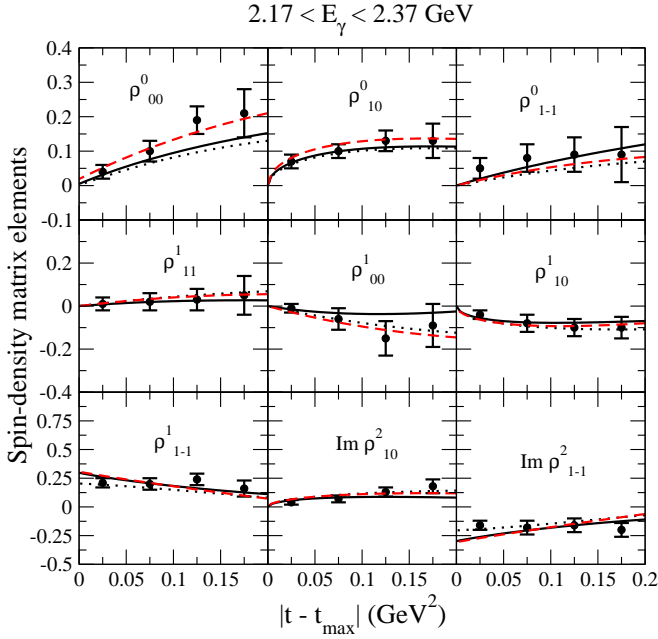


FIG. 8: (Color online) Spin-density matrix elements  $\rho_{ij}^\alpha$  in Gottfried-Jackson system as a function of  $t$  at  $2.17 < E_\gamma < 2.37$  GeV. Notation is as in Fig. 4.

$$W(\Phi + \Psi) = \frac{1}{2\pi} \{1 + 2P_\gamma(\rho_{1-1}^1 + \text{Im}\rho_{1-1}^2)\} \\ \times \cos[2(\Phi + \Psi)],$$

$$W(\Psi) = \frac{1}{2\pi} [1 - P_\gamma(2\rho_{11}^1 + \rho_{00}^1) \cos 2\Psi], \quad (17)$$

where the angles  $\Theta$ ,  $\Phi$ , and  $\Psi$  are illustrated in Fig. 3. Here, they are measured at two different energy bins  $1.97 < E_\gamma < 2.17$  GeV and  $2.17 < E_\gamma < 2.37$  GeV within the range of  $|t - t_{\max}| \leq 0.2 \text{ GeV}^2$  ( $t_{\max} = -|t|_{\min}$ ). In our work, they are calculated at the midpoint of each energy bin  $E_\gamma$  by weighing them with the differential cross section as a function of  $t$

$$W(E_\gamma, \Theta, \Phi, \Psi) = \frac{\int_{t_{\max}-0.2}^{t_{\max}} dt [d\sigma(E_\gamma, t)/dt] W(E_\gamma, t, \Theta, \Phi, \Psi)}{\int_{t_{\max}-0.2}^{t_{\max}} dt [d\sigma(E_\gamma, t)/dt]}. \quad (18)$$

It is important to note that it is misleading to conclude that the effect of the resonance, be it  $3/2^+$  or  $3/2^-$ , is insignificant in most cases. Fig. 9 shows the detail of the composition of the spin-density matrix elements as a function of  $t$  at  $1.97 < E_\gamma < 2.17$  GeV for a  $J^P = 3/2^-$  where the full, dotted, dashed, and dash-dotted lines are the total, nonresonant, resonant, and interference between nonresonant and resonant contributions, respectively. It is obvious that the resonant contributions are not negligible compared to the nonresonant ones. However, the interference contributions are also roughly of the same strength as those of the resonance, and in many cases, of the opposite signs. This would cause the total

contributions to come mainly from the nonresonant contributions only. However, it should be emphasized again, that the resonant contributions are not negligible.

Based on the similarities in their masses and spin-parities, one might wonder whether the  $3/2^-$  resonance found here can be identified as the  $D_{13}(2080)$  as listed in PDG [11]. The coupling constants given Table I can be used to calculate the ratio of the helicity amplitudes  $A_{1/2}$  and  $A_{3/2}$ . However, we cannot determine their magnitudes since we have only the products of the coupling constants  $\gamma NN^*$  and  $\phi NN^*$ . We obtain a value of  $A_{1/2}/A_{3/2} = 1.05$ , while it is  $-1.18$  for  $D_{13}(2080)$ . Although their magnitudes are quite similar, they differ by a sign and we conclude that the resonance postulated here, if exists, cannot be identified with  $D_{13}(2080)$ .

### B. Analysis on the composition of the bump structure

Our results for the forward differential cross sections of the  $J^P = 3/2^\pm$  in Fig. 4 indicate constructive and destructive interferences of nonresonant and resonant amplitudes below and above the peak, respectively. Since the nonresonant amplitude is dominated overwhelmingly by Pomeron amplitude, which is almost completely imaginary, it seems to imply that the sign-changing component of the resonant part must then be also imaginary.

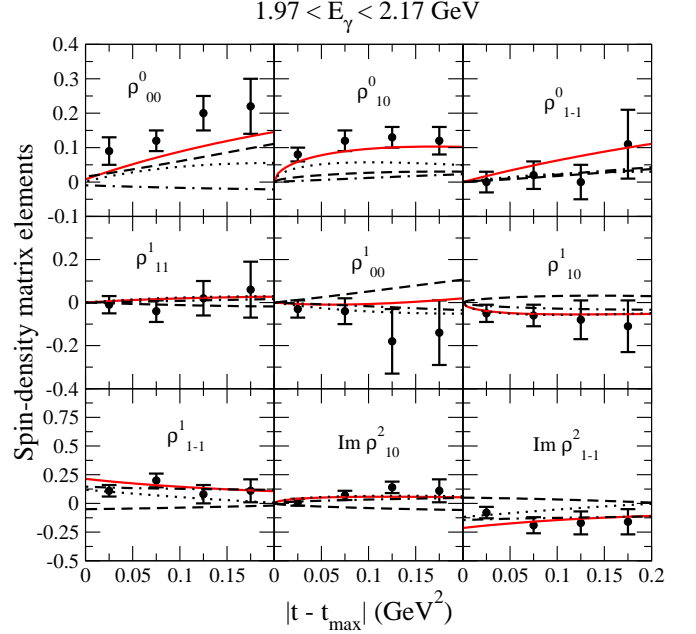


FIG. 9: (Color online) Detail of the composition of spin-density matrix elements  $\rho_{ij}^\alpha$  in Gottfried-Jackson system as a function of  $t$  at  $1.97 < E_\gamma < 2.17$  GeV for a  $J^P = 3/2^-$  resonance. Note that we have different notation here. The full, dotted, dashed, and dash-dotted lines are the total, nonresonant, resonant, and interference between nonresonant and resonant contributions, respectively.

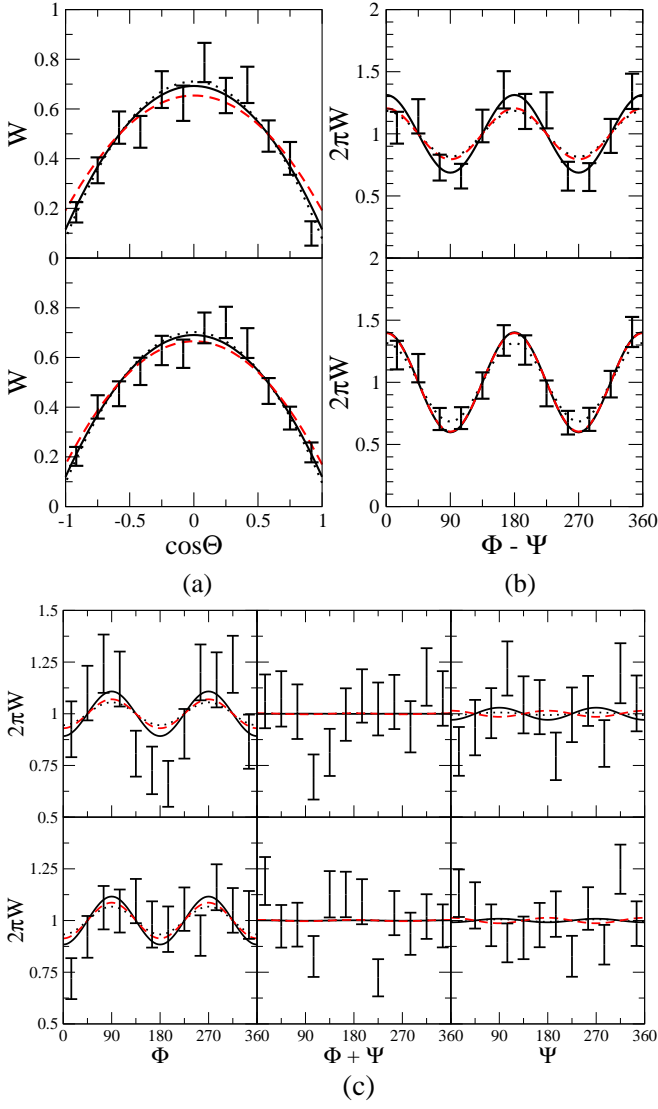


FIG. 10: (Color online) Decay angular distributions (a)  $W(\cos \Theta)$ , (b)  $W(\Phi - \Psi)$ , (c)  $W(\Phi)$ ,  $W(\Phi + \Psi)$ , and  $W(\Psi)$ , at photon LAB energies 1.97 – 2.17 GeV (upper panels) and 2.17 – 2.37 GeV (lower panels) within the range of  $|t - t_{\max}| \leq 0.2$  GeV<sup>2</sup>. Notation is as in Fig. 4.

However, it is well-known that the imaginary part of the resonant amplitude is sign definite while the sign-changing component of a resonant amplitude is real.

In order to understand this, let us decompose the forward differential cross section ( $\propto |T|^2$ ) into its nonresonant, resonant, and interference terms

$$|T|^2 = |T_{NR}|^2 + |T_R|^2 + 2\text{Re}(T_{NR}T_R^*), \quad (19)$$

in which  $T$ ,  $T_{NR}$ , and  $T_R$  are the total, nonresonant, and resonant amplitudes, respectively. We also have

$$T_{NR} = T_P + T_M, \quad (20)$$

where  $T_P$  and  $T_M$  are the Pomeron and meson-exchange amplitude, respectively. The interference term between

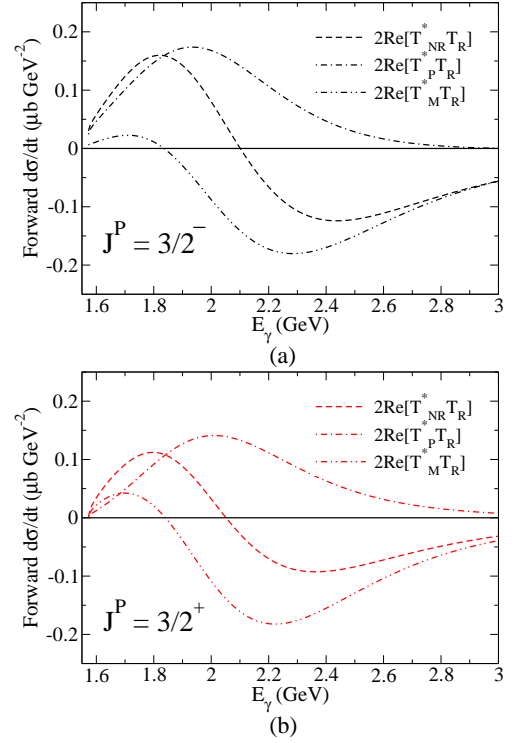


FIG. 11: (Color online) Decomposition of the contribution of the interference between the resonant and nonresonant amplitudes,  $2\text{Re}(T_{NR}T_R^*)$ , to the differential cross section at forward angle as a function of incident photon energy  $E_\gamma$  for a resonance with (a)  $J^P = 3/2^-$  and (b)  $J^P = 3/2^+$ . The dot-dashed, and dot-dot-dashed lines denote the interferences of the resonant amplitude with the pomeron and meson-exchange amplitudes,  $2\text{Re}(T_P T_R^*)$  and  $2\text{Re}(T_M T_R^*)$ , respectively, while the dashed lines represent the sum  $2\text{Re}(T_{NR}T_R^*)$ .

the resonant and nonresonant amplitude  $\text{Re}(T_{NR}T_R^*)$  can be further decomposed into a sum of interference terms between the resonant and pomeron amplitudes  $\text{Re}(T_P T_R^*)$ , and the resonant and meson-exchange amplitudes  $\text{Re}(T_M T_R^*)$ , respectively. This decomposition is shown in the Fig. 11, where the dot-dashed and dot-dot-dashed lines represent  $\text{Re}(T_P T_R^*)$  and  $\text{Re}(T_M T_R^*)$ , respectively, with dashed lines denoting their sum  $\text{Re}(T_{NR}T_R^*)$ . It is seen that for both  $J^P = 3/2^\pm$  resonances,  $\text{Re}(T_P T_R^*)$  is always positive, while  $2\text{Re}(T_M T_R^*)$  turns negative at around  $E_\gamma = 1.82$  GeV and becomes comparable in size to  $\text{Re}(T_P T_R^*)$  such that the sum  $\text{Re}(T_{NR}T_R^*)$  eventually changes sign. We conclude that the meson-exchange mechanisms are indeed crucial in producing the peaking behavior observed in  $\phi$ -photoproduction reaction.

### C. Effects of the postulated resonance in the $\omega N$ channel

We further study the possible effect of this postulated resonance in the  $\omega N$  channel. The conventional "mini-

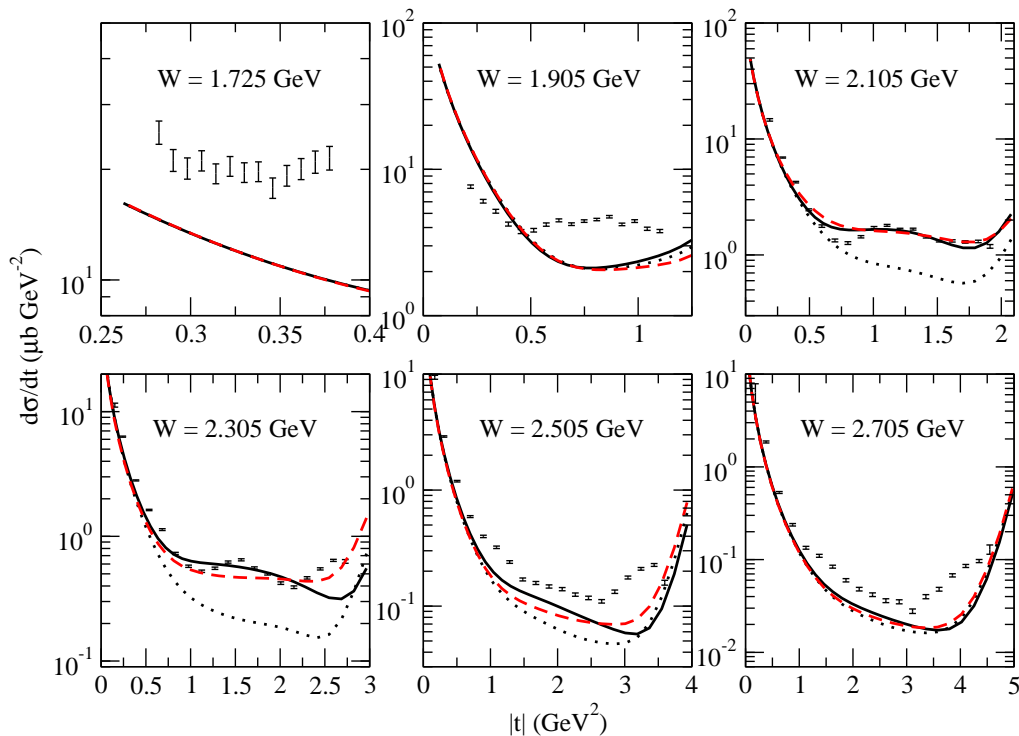


FIG. 12: (Color online) Predictions of the effects of the postulated resonances to the differential cross section of  $\omega$  photoproduction at CM energies  $W$ , as given inside each plot. Data is from Ref. [27]. Notation is as in Fig. 4.

mal" parametrization relating  $\phi NN^*$  and  $\omega NN^*$  is

$$g_{\phi NN^*} = -\tan \Delta\theta_V x_{\text{OZI}} g_{\omega NN^*}, \quad (21)$$

with  $\Delta\theta_V \simeq 3.7^\circ$  corresponding to the deviation from the ideal  $\phi - \omega$  mixing angle. Here,  $x_{\text{OZI}}$  is called the OZI-evading parameter and the larger value of  $x_{\text{OZI}}$  would indicate larger strangeness content of the resonance.

For the present purpose, we choose the  $\omega$  photoproduction model of Ref. [26] which includes the nucleon resonances predicted by Refs. [24, 25]. In Fig. 12, one sees that the prediction of this model for the  $t$ -dependence of differential cross section at  $W = 2.105$  GeV, given in dotted line, exhibits substantial discrepancy with the most recent experimental data [27] for  $|t| > 0.75$  GeV<sup>2</sup>. With the addition of resonance postulated here with  $x_{\text{OZI}} = 12(9)$  for  $J^P = 3/2^- (J^P = 3/2^+)$ , we see that the differential cross section at  $W = 2.105$  and 2.305 GeV, as denoted by the solid black (dashed red) line in Fig. 12, can be reproduced with roughly the correct strength. At the other energies, the improvement is much less noticeable because they are far from the energy of the resonance. The large values of  $x_{\text{OZI}}$  would imply that the resonances we propose here might contain considerable amount of strangeness contents, an issue we now turn to in the next subsection.

#### D. Strangeness content of the postulated resonance

The resonance proposed here appears to have a large OZI evasion parameter  $x_{\text{OZI}}$  which would lead one to ask whether this is reasonable. In this section, we will estimate the strangeness content of the resonance. We can write, for the wavefunction of the resonance [28],

$$|N^*\rangle = x|uud\rangle + z_u|uudu\bar{u}\rangle + z_d|uudd\bar{d}\rangle + z_s|uuds\bar{s}\rangle, \quad (22)$$

where  $x$  is real but  $z_u$ ,  $z_d$ , and  $z_s$  are all complex and  $|x|^2 + |z_u|^2 + |z_d|^2 + |z_s|^2 = 1$ . Let us define

$$Z_{id} \equiv \frac{\mathcal{M}(N^* \rightarrow \phi_{id}N)}{\mathcal{M}(N^* \rightarrow \omega_{id}N)}, \quad (23)$$

where  $\mathcal{M}(N^* \rightarrow V_{id}N)$  is the amplitude of the decay of  $N^*$  to  $V_{id}N$  where the subscript "id" denotes that the

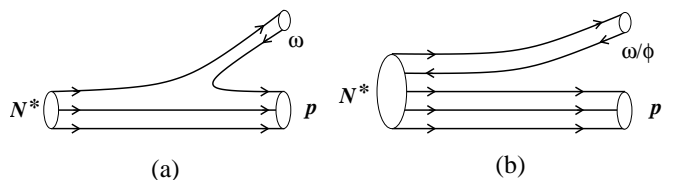


FIG. 13: Quark-flow diagrams of the processes that correspond to the amplitudes (a)  $\mathcal{M}_3$  and (b)  $\mathcal{M}_5$ .

vector meson  $V$  is in its ideal state. For example,  $\phi_{id}$  consists of pure  $s\bar{s}$  with no  $u\bar{u}$  or  $d\bar{d}$  mixture.

We can obtain  $Z_{id}$  experimentally from

$$Z_{id} = \frac{Z_{\text{phys}} + \tan \Delta\theta_V}{1 - Z_{\text{phys}} \tan \Delta\theta_V}, \quad (24)$$

where

$$Z_{\text{phys}} \equiv \frac{\mathcal{M}(N^* \rightarrow \phi N)}{\mathcal{M}(N^* \rightarrow \omega N)}, \quad (25)$$

is defined for the physical particles  $\phi$  and  $\omega$ . Here,  $Z_{\text{phys}}$  can be estimated from  $g_{\phi NN^*}/g_{\omega NN^*} = -x_{\text{OZI}} \tan \Delta\theta_V$ . Notice that  $Z_{id} = 0$  when  $x_{\text{OZI}} = 1$  which corresponds to the case of ordinary OZI violation arising from an  $\omega\phi$  mixing without the presence of strangeness content in the resonance  $N^*$ . By using the values of  $x_{\text{OZI}}$  for the resonance found in this work, the values for their  $Z_{\text{phys}}$  can also be calculated from Eq. (21). Therefore, employing Eq. (24) above, we can obtain the values of  $Z_{id}$ , which are found to be  $-0.68$  and  $-0.50$  for  $J^P = 3/2^-$  and  $J^P = 3/2^+$  resonances, respectively.

Within the constituent quark model,  $Z_{id}$  is related to the amplitudes  $\mathcal{M}_3$  and  $\mathcal{M}_5$  corresponding to the processes depicted in Fig. 13(a) and (b), respectively, as followings

$$\begin{aligned} \mathcal{M}(N^* \rightarrow \phi_{id} N) &= z_s \mathcal{M}_5, \\ \mathcal{M}(N^* \rightarrow \omega_{id} N) &= x \mathcal{M}_3 + \frac{1}{\sqrt{2}} (z_u + z_d) \mathcal{M}_5. \end{aligned} \quad (26)$$

Let us now write  $z_q \equiv \delta_q a_q$ , where  $q = u, d, s$ , which separates the phase factor  $\delta_q = e^{i\theta_q}$  of phase  $\theta_q$  and the magnitude  $a_q = |z_q|$  of the amplitude. We further introduce  $c_u \equiv a_u/a_s$  and  $c_d \equiv a_d/a_s$ . After substituting, we have

$$Z_{id} = \frac{z_s \mathcal{M}_5}{x \mathcal{M}_3 + \frac{1}{\sqrt{2}} (\delta_s^* \delta_u c_u + \delta_s^* \delta_d c_d) z_s \mathcal{M}_5}, \quad (27)$$

which leads to the probability of the strangeness content

$$P_s \equiv |z_s|^2 = \frac{|Z_{id}|^2 |F|^2}{(1 + c_u^2 + c_d^2) |Z_{id}|^2 |F|^2 + |N|^2}, \quad (28)$$

where

$$N \equiv 1 - \frac{1}{\sqrt{2}} Z_{id} (\delta_s^* \delta_u c_u + \delta_s^* \delta_d c_d), \quad (29)$$

$$F \equiv \frac{\mathcal{M}_3}{\mathcal{M}_5}. \quad (30)$$

It is seen that the strangeness probability  $P_s$  depends on  $\mathcal{M}_{3,5}$  and  $z_q$ 's in a complicated way. The problem here is to make an educated estimate of it. Here, we first follow Ref. [29] to assume that  $P_{u,d}/P_s = (m_s/m_{u,d})^2$ . It leads to  $c_u = c_d = m_s/m_{u,d}$  where  $m_s$  and  $m_{u,d}$  will be taken as 0.5 and 0.3 GeV, respectively. To proceed, we further assume the ratio  $|F|$  between the reaction amplitudes

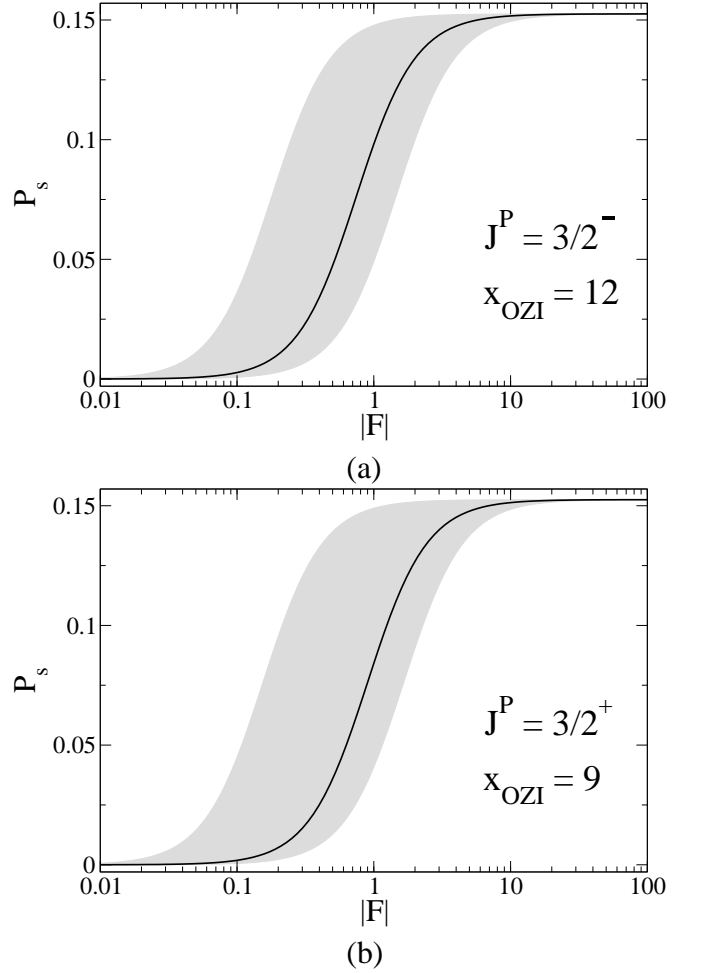


FIG. 14: Strangeness content of the resonances  $P_s$  for  $x_{\text{OZI}} = 12$  and  $x_{\text{OZI}} = 9$  corresponding to (a)  $J^P = 3/2^-$  and (b)  $J^P = 3/2^+$  resonances, respectively, as functions of  $|F|$ . The shaded areas show the 95% probability range after the phases are randomly varied. The solid lines are the median.

$\mathcal{M}_3$  and  $\mathcal{M}_5$  to lie within the range of 0.01 and 100, i.e.,  $|\mathcal{M}_3| = (0.01 \sim 100)|\mathcal{M}_5|$  and find the possible range of  $P_s$ . For a fixed value of  $|F|$ , we randomly vary the phase factors  $\delta_q$ 's to give  $P_s$ . The results, within 95% probability, are given by the shaded area in Fig. 14 while the median values are denoted by the solid lines.

Notice that, for a fixed value of  $|F|$ , the lower bound of  $P_s$  is given by  $|N|_{\text{max}} = 1 + \frac{1}{\sqrt{2}} |Z_{id}| (c_u + c_d)$ , that is, when all the phases are such that the second term in  $N$  of Eq. (29), interferes constructively with the first. The lower bound of  $P_s$  goes to zero like  $|Z_{id}/N_{\text{max}}|^2 |F|^2$  as  $|F|$  approaches zero and approaches  $1/(1 + c_u^2 + c_d^2) = 0.153$  when  $|F|$  grows larger. When  $|N|_{\text{min}} = 0$ , the upper bound of  $P_s = 1/(1 + c_u^2 + c_d^2) = 0.153$  is reached. Note that with the values of  $Z_{id}$  of the resonance given above, the condition  $|N|_{\text{min}} = 0$  can indeed be met with some combinations of the phase factors  $\delta_q$ 's. We point out that  $P_s = 1/(1 + c_u^2 + c_d^2) = 0.153$ , would correspond to a resonance with 100% five-quark content, namely, a

pentaquark state.

A rather broad range of  $P_s$  also reflects the situation faced in the efforts to determine the strangeness content in the proton, which is stable and can be more directly studied. Recent studies give estimates ranging from 0.025 – 0.058% [30] to 2.4 – 2.9% [31].

### E. Polarization observables

Since the fitted results with both assignments  $3/2^\pm$  for the resonance are rather similar, we need to find some observables that can help us to distinguish them. Here, we show some predictions for the polarization observables at photon laboratory energy  $E_\gamma = 2.0$  GeV near the resonance position. Three single polarization observables: asymmetries of the polarized beam  $\Sigma_x$ , polarized target  $T_y$ , and recoil polarization  $P_{y'}$  are given in Fig. 15 while four double polarization observables: beam-target (BT) asymmetries  $C_{yx}^{BT}$ ,  $C_{yz}^{BT}$ ,  $C_{zx}^{BT}$ , and  $C_{zz}^{BT}$ , with the photon beam and the nucleon target polarized, are given in Fig. 16, where the dotted, solid, and dashed lines correspond to the contributions from background only, and with the addition of the postulated resonance of  $J^P = 3/2^-$  and  $J^P = 3/2^+$ , respectively. The notation of the polarization observables follows Ref. [9].

It can be concluded from Figs. 15 and 16 that while all the observables presented are reasonably distinct enough to distinguish the parities of the  $J = 3/2$  resonances, the single polarization observable  $\Sigma_x$  is actually the most distinct based on the opposite sign of the curves produced by the two parities.

## IV. SUMMARY AND CONCLUSIONS

In summary, we present the details and more extensive results of the analysis of the near-threshold bump structure in the forward differential cross section of the  $\phi$ -meson photoproduction to determine whether it is a signature of a resonance. The analysis is carried out with an effective Lagrangian approach which includes Pomeron and  $(\pi, \eta)$  exchanges in the  $t$  channel and contributions from the  $s$ - and  $u$ -channel excitation of a postulated resonance.

Besides the differential cross sections at forward angle as function of photon energy and as function of  $t$ , the recent data on nine spin-density matrix elements at three photon energies reported by the LEPS collaboration are used, instead of the decay angular distributions of the  $\phi$  meson, which depend only on six spin-density matrix elements, as was done before in Ref. [14], to constrain the model. Moreover, the new spin-density matrix element data are given as a function of  $t$ , while the previous decay angular distribution data are not. Therefore, the new set of data are expected to give more strict constraints on the resulting resonance parameters.

We conclude that indeed the nonmonotonic behavior, along with the other experimental data, as reported by LEPS, can only be explained with an assumption of the excitation of a resonance of spin 3/2, as previously reported. However, both parities of  $(\pm)$  can account for the data equally well with almost identical mass of  $2.08 \pm 0.04$  GeV and width of  $0.501 \pm 0.117$  and  $0.570 \pm 0.159$  for  $3/2^-$  and  $3/2^+$ , respectively. Spin-1/2 resonances can still explain the nonmonotonic behavior, but however would lead to large resonance contributions, which would cause differential cross sections as functions of  $t$ , as well as the spin-density matrix elements to disagree with experimental data.

The helicity amplitudes of the  $J^P = 3/2^-$  resonance calculated from the obtained coupling constants gives a ratio of  $A_{1/2}/A_{3/2} = 1.05$  which differs in sign from the value of  $-1.18$  of  $D_{13}(2080)$  given by the PDG. Therefore, we conclude that the  $J^P = 3/2^-$  resonance cannot be identified as  $D_{13}(2080)$ . The ratio of helicity amplitudes of the  $J^P = 3/2^+$  resonance is obtained to be of  $A_{1/2}/A_{3/2} = 0.89$ .

Some of the single and double polarization observables which are sensitive to the parity of the resonance, including beam asymmetry  $\Sigma_x$ , target asymmetry  $T_x$ , recoil asymmetry  $P_x$ , and beam-target asymmetry  $C_{ij}^{BT}$ , near the resonance peak are also given. Measurement of these quantities would be most helpful in further substantiating whether the nonmonotonic behavior is indeed a signature of resonance as well as resolving its parity. We find that the single polarization observable of beam asymmetry  $\Sigma_x$  provides an excellent way to resolve the parity of the resonance since they are of opposite signs with different parity.

We have also investigated the effects of the postulated resonances to the differential cross section of  $\omega$  photoproduction as a function of  $t$  within the model of Ref. [26]. We find that the proposed resonance improves the agreement with the data, especially around the photon LAB energy of 2.1 GeV, if large values of OZI-evading parameter  $x_{\text{OZI}} = 12$  and  $x_{\text{OZI}} = 9$  for  $J^P = 3/2^-$  and  $J^P = 3/2^+$  resonances, respectively, are assumed. Here, again, both resonances are equally capable of improving the discrepancy between the data and the predictions of Ref. [26]. It adds support for the resonance we postulate. We argue that the large values of OZI-evading parameter  $x_{\text{OZI}}$  found imply that the postulated resonance might contain a strangeness content of  $P_s = 0.1 \sim 15\%$ . If the postulated resonance contains considerable amount of strangeness, then it could couple strongly to, say,  $K\Lambda$  channel. Question would then arise on how the coupled-channel effects would modify the low-energy behavior of the nonresonant amplitude employed in this investigation. This can be answered only with a full coupled-channel calculations.

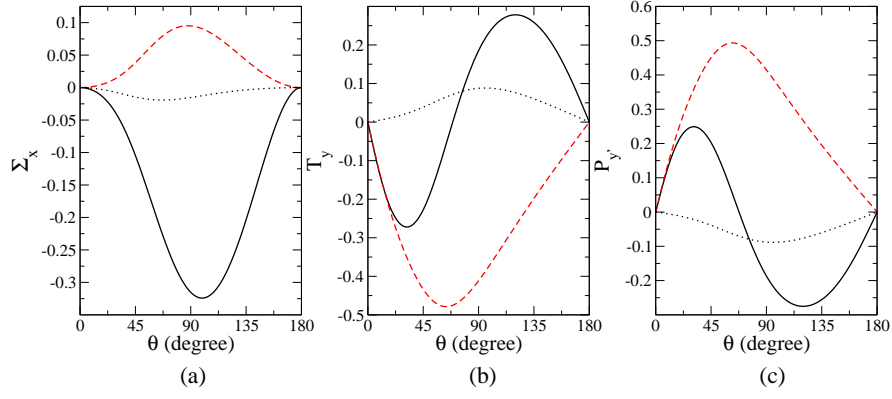


FIG. 15: (Color online) Single polarization observables for  $\gamma p \rightarrow \phi p$  reaction: (a) polarized beam  $\Sigma_x$ , (b) polarized target  $T_y$ , and (c) recoil polarization  $P_{y'}$  asymmetries, taken at photon laboratory energy  $E_\gamma = 2.0$  GeV. The dotted lines denote the background contribution, while the solid black and red lines are contributions from resonances with  $J^P = 3/2^-$  and  $J^P = 3/2^+$ , respectively.

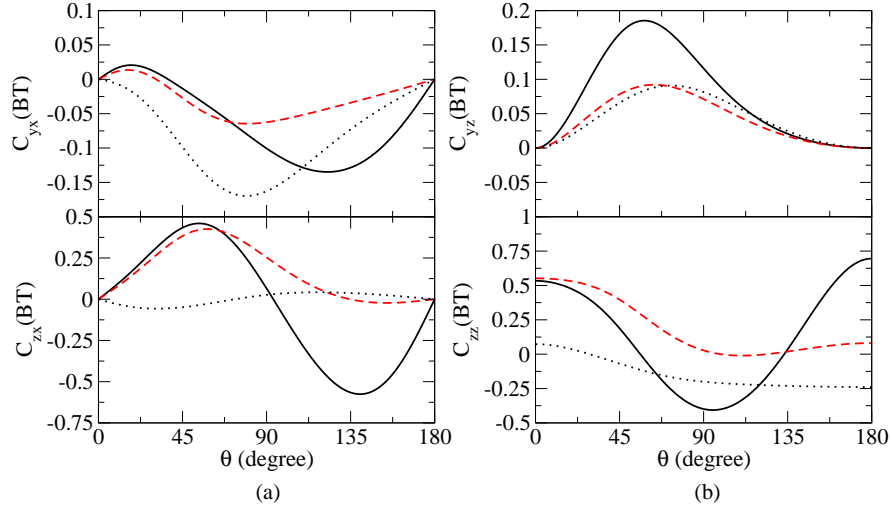


FIG. 16: (Color online) Double polarization observables for  $\gamma p \rightarrow \phi p$  reaction: beam-target (BT) asymmetries (a)  $C_{yx}^{BT}$  and  $C_{zx}^{BT}$ , (b)  $C_{yz}^{BT}$  and  $C_{zz}^{BT}$ , with photon beam and nucleon target polarized, taken at photon laboratory energy  $E_\gamma = 2.0$  GeV. Notation is as in Fig.15.

### Acknowledgments

We would like to thank Drs. W.C. Chang, A.I. Titov, T.-S.H. Lee, and Yongseok Oh for useful discussions and/or correspondences. This work was supported in parts by National Science Council of the Republic

of China (Taiwan) under grant NSC100-2112-M002-012. We would also like to acknowledge the help from National Taiwan University High-Performance Computing Center in providing us with a fast and dependable computation environment which is essential in carrying out this work.

- 
- [1] T. H. Bauer, R. D. Spital, D. R. Yennie and F. M. Pipkin, Rev. Mod. Phys. **50**, 261 (1978).
  - [2] A. Donnachie and P. V. Landshoff, Phys. Lett. B **185**, 403 (1987); Nucl. Phys. B **244**, 322 (1984); Nucl. Phys. B **267**, 690 (1986); Nucl. Phys. B **311**, 509 (1989).
  - [3] R. A. Williams, Phys. Rev. C **57**, 223 (1998).
  - [4] Y. S. Oh and H. C. Bhang, Phys. Rev. C **64**, 055207 (2001).
  - [5] Q. Zhao, J.-P. Didelez, M. Guidal and B. Saghai, Nucl. Phys. A **660**, 323 (1999); Q. Zhao, B. Saghai and J. S. Al-Khalili, Phys. Lett. B **509**, 231 (2001).
  - [6] A. I. Titov, T.-S. H. Lee, Phys. Rev. C **67**, 065205 (2003).
  - [7] A. I. Titov, T.-S. H. Lee, H. Toki, and O. Streltsova, Phys. Rev. C **60**, 035205 (1999).
  - [8] A. I. Titov, Y. S. Oh and S. N. Yang, Phys. Rev. Lett. **79**, 1634 (1997); A. I. Titov, Y. Oh, S. N. Yang, and T.

- Morii, Nucl. Phys. A **684**, 354 (2001).
- [9] A. I. Titov, Y. Oh, S. N. Yang, and T. Morii, Phys. Rev. C **58**, 2429 (1998).
- [10] T. Mibe *et al.* (LEPS Collaboration), Phys. Rev. Lett. **95**, 182001 (2005) and references therein.
- [11] K. Nakamura *et al.* (Particle Data Group), J. Phys. G **37**, 075021 (2010).
- [12] H. J. Besch *et al.*, Nucl. Phys. B **70**, 257 (1974).
- [13] CLAS Collaboration, E. Anciant *et al.*, Phys. Rev. Lett. **85**, 4682 (2000).
- [14] A. Kiswandhi, J.J. Xie, and S.N. Yang, Phys. Lett. B **691**, 214 (2010).
- [15] S. Ozaki, A. Hosaka, H. Nagahiro, and O. Scholten, Phys. Rev. C **80**, 035201 (2009); **81**, 059901(E) (2010).
- [16] W. C. Chang *et al.* (LEPS Collaboration), Phys. Rev. C **82**, 015205 (2010)
- [17] A. I. Titov and B. Kämpfer, Phys. Rev. C **76**, 035202 (2007).
- [18] Durham High Energy Physics database (HEPDATA) (<http://www.slac.stanford.edu/spires/hepdata>).
- [19] W.-T. Chiang, S. N. Yang, M. Vanderhaeghen, and D. Drechsel, Nucl. Phys. A **723**, 205 (2003).
- [20] C.-T. Hung, S.N. Yang, and T.-S.H. Lee, Phys. Rev. C **64**, 034309 (2001).
- [21] V. Pascalutsa, M. Vanderhaeghen, and S. N. Yang, Phys. Rept. **437**, 125 (2007).
- [22] T. Feuster and U. Mosel, Nucl. Phys. A **612**, 375 (1997).
- [23] K. Schilling, K. Seyboth, and G. Wolf, Nucl. Phys. B **15**, 397 (1970).
- [24] S. Capstick and W. Roberts, Phys. Rev. D **49**, 4570 (1994).
- [25] S. Capstick, Phys. Rev. D **46**, 2864 (1992).
- [26] Y. Oh, A. I. Titov, and T.-S.H. Lee, Phys. Rev. C **63**, 025201 (2001).
- [27] M. Williams *et al.*, Phys. Rev. C **80**, 065208 (2009).
- [28] J. Ellis, M. Karliner, D.E. Kharzeev, M.G. Sapozhnikov, Phys. Lett. B **353**, 319 (1995); G. Höhler *et al.*, Nucl. Phys. B **114**, 505 (1976); S. Dubnicka, Nuovo Cimento A **100**, 1 (1988).
- [29] S.J. Brodsky, P. Hoyer, C. Peterson, and N. Sakai, Phys. Lett. B **93**, 451 (1980); S.J. Brodsky, C. Peterson, and N. Sakai, Phys. Rev. D **23**, 2745 (1981).
- [30] A. Kiswandhi, H.-C. Lee, and S.N. Yang, Phys. Lett. B **704**, 373 (2011).
- [31] W.C. Chang and J.C. Peng, Phys. Lett. B **704**, 197 (2011), Phys. Rev. Lett **106**, 252002 (2011).